Multibody Syst Dyn (2013) 30:343–358
DOI 10.1007/s11044-013-9350-2

A Lagrange–Eulerian formulation of an axially moving beam based on the absolute nodal coordinate formulation

Astrid Pechstein · Johannes Gerstmayr

Received: 17 September 2012 / Accepted: 16 January 2013 / Published online: 30 January 2013

Abstract In the scope of this paper, a finite-element formulation for an axially moving beam is presented. The beam element is based on the absolute nodal coordinate formulation, where position and slope vectors are used as degrees of freedom instead of rotational parameters. The equations of motion for an axially moving beam are derived from generalized Lagrange equations in a Lagrange–Eulerian sense. This procedure yields equations which can be implemented as a straightforward augmentation to the standard equations of motion for a Bernoulli–Euler beam. Moreover, a contact model for frictional contact between an axially moving strip and rotating rolls is presented. To show the efficiency of the method, simulations of a belt drive are presented.

Keywords Absolute nodal coordinate formulation · Axially moving beam · Arbitrary Lagrange Eulerian

1 Introduction

The present paper deals with the simulation of an axially moving strip using beam finite elements with a constant superimposed axial velocity. In contrast to conventional, straightforward computations involving axially transported strips, the considered beam finite elements do not move along the strip axis during the simulation, but keep a fixed undeformed configuration in time. To account for the inertia forces stemming from the transport of mass through the beam element, according terms are added to the standard equations of motion. With this technique, stationary solutions in the pre-critical velocity range can be computed by a quasi-static computation, which is much less time-consuming than a corresponding

A. Pechstein (✉)
Institute of Technical Mechanics, Johannes Kepler University Linz, Altenbergerstr. 69, 4040 Linz, Austria
e-mail: astrid.pechstein@jku.at

J. Gerstmayr
Austrian Center of Competence in Mechatronics, Altenbergerstr. 69, 4040 Linz, Austria
e-mail: johannes.gerstmayr@accm.co.at

transient simulation using a time integration scheme. To include dynamic effects such as vibrations or flutter of the strip, a time-dependent scheme is used. Additionally, a contact formulation for modeling the frictional contact between an axially moving strip and rotating rolls is presented. As a major benefit, in contact computations the elements do not move along the strip but keep a fixed reference configuration. The definition of contact surfaces is alleviated greatly, also in the dynamic case contact surfaces can be assumed fixed throughout the computation, and can easily be resolved by a finer finite-element discretization of the strip.

The finite element developed in this work is based on the absolute nodal coordinate formulation (ANCF) introduced by Shabana [8], which is suitable for large deformation elements. Elements based on the ANCF are characterized by the usage of slope vectors instead of rotational parameters as degrees of freedom. This fact allows the exact representation of inertia of a rigid body. As a major advantage of ANCF elements, their constant mass matrix is often cited. The thickness of the strip under consideration is much smaller than its length, thus Bernoulli–Euler beam theory is applicable. Berzeri and Shabana [3] presented a third order Bernoulli–Euler ANCF beam finite element. Gerstmayr and Irschik [5] modified the equations of virtual work for this element such that it is consistent with the classical theory of extensible Euler elastica. The axially moving element developed in the present paper is based on the element given in the latter reference. For the third order ANCF element, nodal positions and slope vectors are used as degrees of freedom. This ensures continuous differentiability of the beam axis across element borders, which is feasible in applications involving sliding contact.

There exists a vast literature on axially moving continua. A fundamental study was presented by Wickert and Mote [14]. Based on the shear deformable beam by Simo and Vu-Quoc [9], Vu-Quoc and Li [13] derived equations of motion for an axially moving beam. They considered the "sliding spaghetti problem" as a model problem, where a cantilever beam is retrieved into a clamped opening. Behdinan et al. [1, 2] present a related theory under the assumptions of Bernoulli–Euler theory. A formulation for an axially moving Bernoulli–Euler beam transported over a free span is provided by Humer and Irschik [6]. In their setting, the length of the reference configuration is not known in advance. Spelsberg-Korspeter, Kirillov and Hagedorn [11] treat a contact problem of an axially moving beam, which is sliding through rigid brake pads.

The axially moving ANCF element presented in this work is based on a Lagrange–Eulerian approach, also known as arbitrary Lagrangian–Eulerian (ALE) technique. Here, the given constant axial velocity is treated in an Eulerian context, where mass is going through the finite element. While the according Lagrangian reference configuration is moving through the strip in negative direction at the given velocity, the corresponding Eulerian "intermediate configuration" is fixed in space. This notion of intermediate configuration was already mentioned by Vu-Quoc and Li [13] and Behdinan et al. [1]. In their works, the equations of motion were first deduced with respect to the time-dependent Lagrangian reference configuration, and then transformed to the Lagrange–Eulerian case. On the contrary, in the present paper an extended form of Lagrange's equations, which was introduced by Irschik and Holl [7], is used for the derivation of the equations of motion. A similar procedure was suggested by Stangl, Gerstmayr and Irschik [12] for pipe elements, where fluid is transported through the beam element in axial direction. The proposed Lagrange–Eulerian approach leads to a structurally different, but equivalent formulation for a Bernoulli–Euler beam as given in [1]. The presented equations can easily be implemented within the framework of the chosen ANCF finite elements. For the fixed Eulerian configuration, also the computation of the work of elastic forces is greatly simplified.

In applications, contact between the axially moving strip and fixed, moving or rotating bodies may arise. In case of frictional contact, the contact conditions have to be rewritten to account for superimposed relative movements of strip and objects. A contribution in this field from Spelsberg-Korspeter, Kirillov and Hagedorn [11] treats a frictional contact problem of an axially moving beam, which is sliding through rigid brake pads. In the current paper, contact between strip and rolls is considered. The application of Coulomb's law of contact leads to special friction conditions for this case. Since the strip elements do not move according to the axial velocity, but have a fixed Eulerian reference configuration, the definition of contact surfaces is alleviated greatly. The finite-element mesh can be defined adaptively, using a fine discretization in contact areas, and coarser elements in the free-span regions between the rolls. In a comparable fully Lagrangian dynamic formulation, the contact surfaces change rapidly in time, and small elements have to be used for the whole belt geometry, which leads to higher computational effort and simulation times.

As an application, the simulation of a belt drive is considered. A dynamic setup is chosen for the computation. Two different simulations are compared: one using standard ANCF Bernoulli–Euler elements, and one employing the proposed elements with prescribed axial velocity. When using the new technique, the elements discretizing the belt keep a fixed configuration in time, which alleviates the definition of contact surface, and allows for an adaptive discretization of the strip. Thus, the computational effort of the simulation can be reduced greatly, while the accuracy of the solution is maintained.

The present paper is an extension of a work presented by the authors at the Seventh International Conference on Engineering Computational Technology, [10].

2 A beam element with prescribed axial velocity based on the absolute nodal coordinate formulation

In the following, a Bernoulli–Euler beam finite element with prescribed, constant axial velocity is presented. It is derived from the third-order planar ANCF beam finite element introduced by Gerstmayr and Irschik [5]. Throughout the following, the length of the beam element in undeformed configuration is denoted by L, while H is the thickness in vertical direction, and W is the width in direction orthogonal to the xy-plane. The element will be presented in detail in the following, see Fig. 2 for a sketch. For a rectangular cross section, the area of the cross section is given by $A = H \cdot W$ and the second moment of area is $I = W\frac{H^3}{12}$.

The Lagrangian reference configuration of the finite element is moving through the strip opposite to the local ξ axis at the prescribed velocity v_0, see Fig. 1. However, for the sake of simplicity of elastic forces, inertia terms and contact conditions are computed with respect to an "intermediate configuration", which is fixed in space. This concept of a spatially fixed reference system was also used in [1, 13]. In the following, $\bar{x} \in [-L/2, L/2]$ shall denote the position on the undeformed beam axis in the spatially fixed intermediate configuration, while ξ corresponds to the axial position with respect to the moving Lagrangian reference configuration. In Fig. 1, both the moving Lagrangian reference configuration with axial coordinate ξ and the spatially fixed intermediate configuration with axial coordinate $\bar{x}$ are displayed. At time t, these two coordinates are related via a shift of length $v_0 t$,

$$\bar{x} = \bar{x}(\xi, t) = \xi + v_0 t. \tag{1}$$

Let $\mathbf{r} = [r_x \; r_y]^T$ denote the position vector of the beam center line, see Fig. 2. The position vector will be regarded as a function of the spatial axial coordinate $\bar{x}$ and time t, i.e. $\mathbf{r} =$

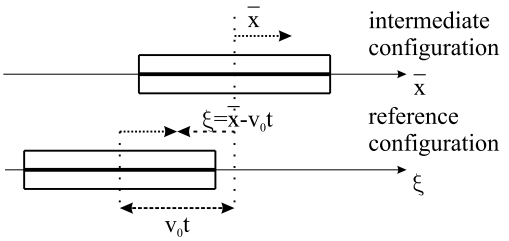

Fig. 1 While the Lagrangian reference configuration is moving in negative direction relative to the local ξ axis at the given velocity, the intermediate configuration is fixed in space

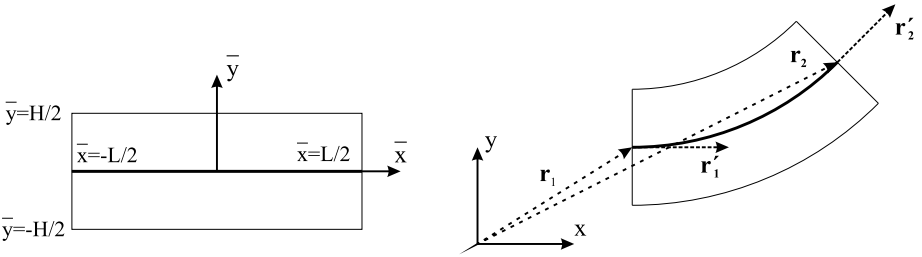

Fig. 2 Axially moving ANCF element: Eulerian (intermediate) reference configuration and deformed element. Degrees of freedom are position and slope vectors of the beam axis in the end points

$\mathbf{r}(\bar{x}, t)$. Let $\mathbf{r}'$ and $\dot{\mathbf{r}}$ be the derivatives with respect to the spatial coordinate $\bar{x}$ and time t, respectively

$$\mathbf{r}' = \frac{\partial \mathbf{r}}{\partial \bar{x}} \quad \text{and} \quad \dot{\mathbf{r}} = \frac{\partial \mathbf{r}}{\partial t}. \tag{2}$$

In the framework of Bernoulli–Euler theory it is assumed that the cross section of the beam is rigid and normal to the beam axis. Thus, a point at distance $\bar{y} \in [-H/2, H/2]$ from the beam axis in the undeformed configuration has the position vector

$$\mathbf{p}(\bar{x}, \bar{y}) = \mathbf{r}(\bar{x}) + \bar{y}\mathbf{n}(\bar{x}). \tag{3}$$

Here $\mathbf{n}$ denotes the (normalized) normal to the beam axis, while $\mathbf{t}$ is the (normalized) tangential vector

$$\mathbf{t}(\bar{x}) = \frac{1}{|\mathbf{r}'|}\begin{bmatrix} r'_x \\ r'_y \end{bmatrix} \quad \text{and} \quad \mathbf{n}(\bar{x}) = \mathbf{t}(\bar{x})^{\perp} = \frac{1}{|\mathbf{r}'|}\begin{bmatrix} -r'_y \\ r'_x \end{bmatrix}. \tag{4}$$

Here and in the following, $\mathbf{a}^{\perp}$ is the rotation of a vector $\mathbf{a}$ by 90° according to the implicit definition in Eq. (4).

Due to the relationship (1), the position vector can also be given as function of the material (Lagrangian) axial coordinate ξ and time t, $\mathbf{r}(\xi, t) = \mathbf{r}(\bar{x}(\xi, t), t)$. The velocity $\mathbf{v}(\bar{x}, t)$ of a point on the beam axis is given by the time derivative of the position vector defined in the Lagrangian reference configuration,

$$\mathbf{v}(\bar{x}, t) = \frac{\partial}{\partial t}\big(\mathbf{r}\big(\bar{x}(\xi, t), t\big)\big). \tag{5}$$

Due to the chain rule, one obtains

$$\mathbf{v}(\bar{x},t)=\frac{\partial \mathbf{r}}{\partial \bar{x}}(\bar{x},t)\frac{\partial \bar{x}}{\partial t}(\xi,t)+\frac{\partial \mathbf{r}}{\partial t}(\bar{x},t)=v_0\mathbf{r}'(\bar{x},t)+\dot{\mathbf{r}}(\bar{x},t). \tag{6}$$

Therefore, the velocity vector $\mathbf{v}$ does not only depend on $\dot{\mathbf{r}}$, but also on the spatial derivative $\mathbf{r}'$. In the quasi-static case, when the time derivative $\dot{\mathbf{r}}$ vanishes, the velocity vector becomes

$$\mathbf{v}=v_0\mathbf{r}'=v_0|\mathbf{r}'|\mathbf{t}. \tag{7}$$

Thus, the axial velocity $\mathbf{v}$ depends on the given axial velocity v_0 as well as on the axial stretch $|\mathbf{r}'|$. For an unstretched element with $|\mathbf{r}'|=1$, the total axial velocity equals the prescribed velocity v_0 in tangent direction.

The proposed beam finite element is derived from Bernoulli–Euler elements based on the absolute nodal coordinate formulation (ANCF) [3, 5]. The considered ANCF element is depicted in Fig. 2. The degrees of freedom for this element are the positions and slopes of the beam center line at the two nodes of the beam element. This ensures the continuity of gradients along the center line, which is advantageous in applications with sliding contact.

In the considered beam finite element, the position vector $\mathbf{r}$ is interpolated by third order polynomials. For the shape function matrix $\mathbf{S}$ and the element coordinate vector $\mathbf{q}$, the position vector is given by the relationship

$$\mathbf{r}=\mathbf{S}\mathbf{q}. \tag{8}$$

Degrees of freedom of the element are the positions and slopes of the beam center line in the nodal end points. Thus, each node N_j is associated to four generalized coordinates, which are given by

$$\mathbf{q}^{(j)}=\begin{bmatrix}\mathbf{r}|_{N_j}\\ \mathbf{r}'|_{N_j}\end{bmatrix}. \tag{9}$$

For an element with nodes N_{j_1} and N_{j_2}, the generalized element coordinates are

$$\mathbf{q}=\begin{bmatrix}\mathbf{q}^{(j_1)}\\ \mathbf{q}^{(j_2)}\end{bmatrix}. \tag{10}$$

The shape function matrix $\mathbf{S}$ is of the form

$$\mathbf{S}=[S_1\mathbf{I}\quad S_2\mathbf{I}\quad S_3\mathbf{I}\quad S_4\mathbf{I}], \tag{11}$$

where $\mathbf{I}$ denotes the 2×2 unit matrix, and the shape functions S_i are given by

$$S_1(\bar{x})=\frac{1}{2}-\frac{3\bar{x}}{2L}+\frac{2\bar{x}^3}{L^3},\qquad S_2(\bar{x})=\frac{L}{8}-\frac{\bar{x}}{4}-\frac{\bar{x}^2}{2L}+\frac{\bar{x}^3}{L^2}, \tag{12}$$

$$S_3(\bar{x})=\frac{1}{2}+\frac{3\bar{x}}{2L}-\frac{2\bar{x}^3}{L^3},\qquad S_4(\bar{x})=-\frac{L}{8}-\frac{\bar{x}}{4}+\frac{\bar{x}^2}{2L}+\frac{\bar{x}^3}{L^2}. \tag{13}$$

The ith column of $\mathbf{S}$, which corresponds to the shape function for the coordinate q_i, shall be denoted by $\mathbf{S}_i$. This implies that

$$\mathbf{r}=\sum_{i=1}^{8}\mathbf{S}_i q_i\quad\text{and}\quad\frac{\partial \mathbf{r}}{\partial q_i}=\frac{\partial \dot{\mathbf{r}}}{\partial \dot{q}_i}=\mathbf{S}_i. \tag{14}$$

3 Kinetic energy of the axially moving beam element

In [7], Irschik and Holl introduced the Lagrange equations of motion for systems containing non-material volumes, which read in the general case of a volume V

$$\frac{d}{dt}\frac{\partial T}{\partial \dot{q}_i} - \frac{\partial T}{\partial q_i} + \int_S d\mathbf{a} \cdot (\mathbf{v}_0 - \mathbf{w}_0)\frac{\partial T'}{\partial \dot{q}_i} - \int_S d\mathbf{a} \cdot \frac{\partial(\mathbf{v}_0 - \mathbf{w}_0)}{\partial \dot{q}_i} T' = \frac{\partial W_I}{\partial q_i} + \frac{\partial W_E}{\partial q_i}. \tag{15}$$

Therein, $\mathbf{v}_0$ denotes the impressed velocity of the non-material volume, while $\mathbf{w}_0$ is the velocity of the material volume. Moreover, T denotes the total kinetic energy of the system, and T' is the kinetic energy per unit volume,

$$T = \frac{1}{2}\int_V \rho \mathbf{v}^T \mathbf{v}\, dV, \tag{16}$$

$$T' = \frac{1}{2}\rho A \mathbf{v}^T \mathbf{v}. \tag{17}$$

Additionally, W_I is the strain energy due to internal elastic forces, while W_E is the energy corresponding to external forces. The surface of V where mass enters and exits the system is denoted by S. For this surface, let $\mathbf{a}$ be the oriented surface normal vector, while $d\mathbf{a}$ represents an oriented surface element on S.

In the following, the equations of motion (15) are evaluated for V being the intermediate reference configuration of the axially moving ANCF element. Here, the velocity of the material volume $\mathbf{w}_0$ vanishes, since the intermediate configuration of the element is fixed in time, while the velocity vector of the non-material volume $\mathbf{v}_0$ is of absolute value v_0 and points in tangent direction,

$$\mathbf{v}_0 = v_0 \mathbf{t} \quad \text{and} \quad \mathbf{w}_0 = 0. \tag{18}$$

The surfaces S where mass enters and exits the system are the cross sections at the nodal end points of the beam element. Using representation (6) of the velocity vector $\mathbf{v}$, the total kinetic energy T and kinetic energy per unit volume T' transform to

$$T = \frac{1}{2}\int_{-L/2}^{L/2} \rho A \left(v_0 \mathbf{r}' + \dot{\mathbf{r}}\right)^T \left(v_0 \mathbf{r}' + \dot{\mathbf{r}}\right) d\bar{x}, \tag{19}$$

$$T' = \frac{1}{2}\rho A \left(v_0 \mathbf{r}' + \dot{\mathbf{r}}\right)^T \left(v_0 \mathbf{r}' + \dot{\mathbf{r}}\right). \tag{20}$$

All terms in the equations of motion (15) are evaluated separately in Sect. 3.1. In Sect. 3.2 formulae for the quasi-static case are provided, where the time derivative $\dot{\mathbf{r}}$ disappears.

3.1 Equations of motion in the dynamic case

Examining the first term in the Lagrange equations of motion (15) $\frac{d}{dt}\frac{\partial T}{\partial \dot{q}_i}$ leads to

$$\frac{d}{dt}\frac{\partial T}{\partial \dot{q}_i} = \frac{d}{dt}\int_{-L/2}^{L/2} \rho A \left(v_0 \mathbf{r}' + \dot{\mathbf{r}}\right)^T \frac{\partial (v_0 \mathbf{r}' + \dot{\mathbf{r}})}{\partial \dot{q}_i} d\bar{x} \tag{21}$$

$$= \frac{d}{dt}\int_{-L/2}^{L/2} \rho A \left(v_0 \mathbf{r}' + \dot{\mathbf{r}}\right)^T \mathbf{S}_i\, d\bar{x} \tag{22}$$

$$= \int_{-L/2}^{L/2} \rho A \left(v_0 \dot{\mathbf{r}}' + \ddot{\mathbf{r}}\right)^T \mathbf{S}_i \, d\bar{x}. \tag{23}$$

The relations $\partial \dot{\mathbf{r}} / \partial \dot{q}_i = \mathbf{S}_i$ and $\partial \mathbf{r}' / \partial \dot{q}_i = 0$ have been applied in Eq. (21).

The partial derivative of the kinetic energy with respect to q_i yields

$$\frac{\partial T}{\partial q_i} = \int_{-L/2}^{L/2} \rho A \left(v_0 \mathbf{r}' + \dot{\mathbf{r}}\right)^T \frac{\partial (v_0 \mathbf{r}' + \dot{\mathbf{r}})}{\partial q_i} \, d\bar{x} \tag{24}$$

$$= \int_{-L/2}^{L/2} \rho A v_0 \left(v_0 \mathbf{r}' + \dot{\mathbf{r}}\right)^T \mathbf{S}_i' \, d\bar{x}. \tag{25}$$

Next, the surface integrals from Eq. (15) are evaluated. To this end, the partial derivative of the kinetic energy per unit length with respect to the ith generalized velocity $\dot{q}_i$ is computed,

$$\frac{\partial T'}{\partial \dot{q}_i} = \rho A \left(v_0 \mathbf{r}' + \dot{\mathbf{r}}\right)^T \frac{\partial (v_0 \mathbf{r}' + \dot{\mathbf{r}})}{\partial \dot{q}_i} = \rho A \left(v_0 \mathbf{r}' + \dot{\mathbf{r}}\right)^T \mathbf{S}_i. \tag{26}$$

Thus, the first surface integral in Eq. (15) evaluates to

$$\int_S d\mathbf{a} \cdot v_0 \mathbf{t} \frac{\partial T'}{\partial \dot{q}_i} = \int_S d\mathbf{a} \cdot \mathbf{t} \, \rho A v_0 \left(v_0 \mathbf{r}' + \dot{\mathbf{r}}\right)^T \mathbf{S}_i \tag{27}$$

$$= (\mathbf{a} \cdot \mathbf{t}) \rho A v_0 \left(v_0 \mathbf{r}' + \dot{\mathbf{r}}\right)^T \mathbf{S}_i \big|_{\bar{x} = \pm \frac{L}{2}}. \tag{28}$$

In the considered beam element, the scalar product of the oriented surface vector $\mathbf{a}$ and the tangent vector $\mathbf{t}$ yields either minus or plus one, depending whether S is an in- or outflow surface, respectively. On the inflow surface $\bar{x} = -L/2$, we have $\mathbf{a} \cdot \mathbf{t} = -1$, on the outflow surface $\bar{x} = L/2$, we have $\mathbf{a} \cdot \mathbf{t} = 1$. At interfaces where two axially moving beam elements meet, these surface integrals cancel out, since all quantities are continuous across element interfaces.

In the current setup, the given axial velocity vector $v_0 \mathbf{t}$ does not depend on the generalized velocities $\dot{q}_i$. Thus, $\frac{\partial (v_0 \mathbf{t})}{\partial \dot{q}_i} = 0$, and the second surface integral vanishes.

Summing up the representations of the various terms in the generalized Lagrange equations (15), one obtains the following system of equations:

$$\int_{-L/2}^{L/2} \rho A \left(v_0 \dot{\mathbf{r}}' + \ddot{\mathbf{r}}\right)^T \mathbf{S}_i \, d\bar{x} - \int_{-L/2}^{L/2} \rho A v_0 \left(v_0 \mathbf{r}' + \dot{\mathbf{r}}\right)^T \mathbf{S}_i' \, d\bar{x}$$

$$+ \rho A v_0 \left(v_0 \mathbf{r}' + \dot{\mathbf{r}}\right)^T \mathbf{S}_i \big|_{-L/2}^{L/2} = \frac{\partial W_I}{\partial q_i} + \frac{\partial W_E}{\partial q_i}. \tag{29}$$

The authors note that Eq. (29) can be transformed to the set of equations derived by Behdinan and co-workers [1]. To this end, an integration by parts for the second integral in Eq. (29) has to be carried out, which leads to canceling of the surface terms. After regrouping the remaining terms, the system from Eq. (29) reads

$$\int_{-L/2}^{L/2} \rho A \left(2 v_0 \dot{\mathbf{r}}' + \ddot{\mathbf{r}} + v_0^2 \mathbf{r}''\right)^T \mathbf{S}_i \, d\bar{x} = \frac{\partial W_I}{\partial q_i} + \frac{\partial W_E}{\partial q_i}. \tag{30}$$

This is a variational formulation for [1, Eqs. (62)–(63)] in the case of v_0 being constant in time.

3.2 Equations of motion in the quasi-static case

Additionally, the stationary case is considered, in which the time derivative $\dot{\mathbf{r}}$ vanishes. In this case, $\dot{\mathbf{r}}'$ and $\ddot{\mathbf{r}}$ and also the generalized velocities $\dot{q}_i$ disappear. The generalized Lagrange equations evaluated for the dynamic case Eq. (29) reduce to

$$-\int_{-L/2}^{L/2} \rho A v_0^2 \left(\mathbf{r}'\right)^T \mathbf{S}_i' \, d\bar{x} + \rho A v_0^2 \left(\mathbf{r}'\right)^T \mathbf{S}_i \big|_{-L/2}^{L/2} = \frac{\partial W_I}{\partial q_i} + \frac{\partial W_E}{\partial q_i}. \tag{31}$$

4 Generalized elastic forces

The definition of generalized elastic forces is done along the theory presented in [5], where an ANCF Bernoulli–Euler beam element is treated. There, it is proposed to use the nominal or Biot strain tensor, which is defined by

$$\mathbf{E}^{\text{Biot}} = \left(\nabla \mathbf{r}^T \nabla \mathbf{r}\right)^{1/2} - \mathbf{I}. \tag{32}$$

For a Bernoulli–Euler beam, all components but the xx-component ε_{xx} of the Biot strain tensor $\mathbf{E}^{\text{Biot}}$ vanish,

$$\mathbf{E}^{\text{Biot}} = \varepsilon_{xx} \mathbf{e}_x \otimes \mathbf{e}_x. \tag{33}$$

Biot's strain can be split additively into axial strain ε_{ax} and the bending strain $-yK$,

$$\varepsilon_{xx} = \varepsilon_{ax} - yK. \tag{34}$$

The axial strain ε_{ax} is defined as the absolute change of length of the beam axis,

$$\varepsilon_{ax} = \sqrt{\mathbf{r}^T \mathbf{r}} - 1. \tag{35}$$

The bending strain is defined as the negative first moment of Biot's strain, and is related to the material measure of curvature K,

$$K = \frac{\mathbf{r}' \times \mathbf{r}''}{|\mathbf{r}'|^2}. \tag{36}$$

The material measure of curvature differs from the geometrical curvature κ by a factor $|\mathbf{r}'|$,

$$K = |\mathbf{r}'| \kappa. \tag{37}$$

The above definitions lead to the strain energy W_I proposed by [5], which reads

$$W_I = \frac{1}{2} \int_{-L/2}^{L/2} \left(EA\varepsilon_{ax}^2 + EIK^2\right) dx. \tag{38}$$

Here, EA is the axial stiffness, while EI is the bending stiffness including the second moment of area. The generalized forces follow from differentiation of Eq. (38) with respect to the coordinates q_i,

$$\frac{\partial W_I}{\partial q_i} = \int_{-L/2}^{L/2} \left(EA\varepsilon_{ax} \frac{\partial \varepsilon_{ax}}{\partial q_i} + EIK \frac{\partial K}{\partial q_i} \right) d\bar{x}. \tag{39}$$

5 Contact model for the axially moving beam

In many applications, the simulation of an axially moving beam being in contact with other moving or fixed parts of the geometry is of interest. Spelsberg-Korspeter et al. [11] considered the case of an axially moving beam sliding through two brake pads. In the paper at hand, frictional contact of the axially moving strip and rigid rolls shall be regarded.

The rolls are modeled as rigid bodies with fixed center point. The frictional contact force is defined via the relative velocity of roll and strip. In case of a quasi-static computation, it is assumed that the constant roll velocity is prescribed, while for dynamic computations the roll velocity is explicitly computed in the time-dependent scheme. In both cases, the velocities at the roll surface and at the beam element surface are used for the computation of the relative contact velocity, and thereby for the evaluation of contact forces. For quasi-static computations, the rotation of the roll is given explicitly via the prescribed roll velocity. Thus, it is no degree of freedom of the system, but included in the contact formulation.

In the sequel, frictional contact between a single roll and the axially moving strip shall be considered. The roll is characterized by its center point $\mathbf{m}$, its radius r and its angular velocity ω. The tangential contact is governed by Coulomb's law of friction, with the friction coefficient denoted by μ. For each element, two contact points are chosen on the contact surface. These contact points are defined at axial coordinates $\bar{x} = -L/4$ and $\bar{x} = L/4$. The contact conditions will be checked in these points, and contact forces will be applied there.

For the sake of simplicity, the following roll setup is chosen: The roll rotates counterclockwise in positive direction. Thus, angular velocity ω of the roll is always positive. The strip lies below the roll, and runs from the left to the right hand side. Thus, the contact points of an element are chosen at the local coordinates $(\bar{x}_{c,1}, \bar{y}_{c,1}) = (-L/4, H/2)$ and $(\bar{x}_{c,2}, \bar{y}_{c,2}) = (L/4, H/2)$. The setup is displayed in Fig. 3.

5.1 Contact normal force

Modeling the normal contact of roll and axially moving strip can be done in a straightforward manner, the definition of the contact normal force does not differ from well-known contact formulations for finite elements without prescribed axial velocities. In the current approach, a linear contact model with contact stiffness c_c is used, where the contact normal force is proportional to the depth of penetration.

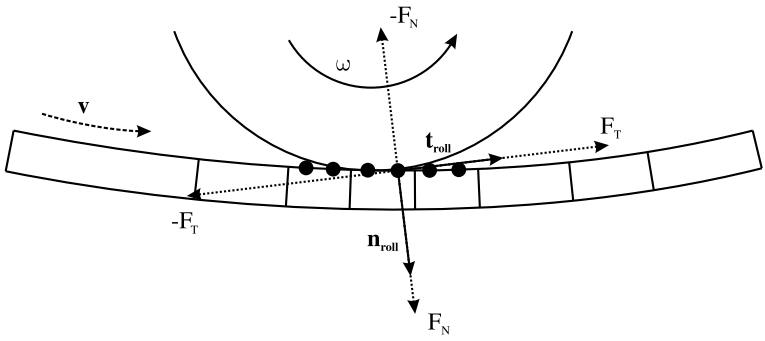

Fig. 3 Setup for the contact between rotating roll and axially moving strip. The roll is rotating in positive direction, the strip is running from left to right. In contact points, contact forces $\mathbf{F}_N$ and $\mathbf{F}_T$ are applied to the strip, negative reaction forces to the roll

Let $(\bar{x}_c, \bar{y}_c)$ be the local coordinates of the considered contact point. Its global position is given by

$$\mathbf{p}_c = \mathbf{p}(\bar{x}_c, \bar{y}_c) = \mathbf{r}(\bar{x}_c) + \bar{y}_c \mathbf{n}(\bar{x}_c). \tag{40}$$

Then, the gap between this contact point and roll is computed as

$$g = |\mathbf{p}_c - \mathbf{m}| - r. \tag{41}$$

The contact normal force is applied in radial direction of the roll $\mathbf{n}_{\text{roll}}$ given by

$$\mathbf{n}_{\text{roll}} := \frac{1}{|\mathbf{p}_c - \mathbf{m}|}(\mathbf{p}_c - \mathbf{m}). \tag{42}$$

For a positive gap, no contact between roll and strip occurs, thus no contact force is imposed. In case of the gap g being negative, a contact force $\mathbf{f}_N$ is applied in radial direction of the roll,

$$\mathbf{f}_N = \begin{cases} -c_c \cdot g \mathbf{n}_{\text{roll}} & \text{if } g < 0, \\ 0 & \text{else.} \end{cases} \tag{43}$$

The corresponding contact normal force $\mathbf{F}_N$ is determined by multiplying the contact pressure with the contact area A_c,

$$\mathbf{F}_N = A_c \mathbf{f}_N \quad \text{with } A_c = \frac{WL}{2}. \tag{44}$$

The corresponding negative contact force $-\mathbf{F}_N$ is applied to the roll.

5.2 Frictional contact forces

The case of frictional contact with a roll is considered in the sequel. In case of quasi-static computations, the angular velocity of the roll is assumed to be of a given, fixed value. For dynamic simulations, the angular velocity of the roll is available in a time stepping scheme. Coulomb's law of friction is applied, which states that the tangential contact force $\mathbf{F}_T$ is bounded by the coefficient of friction μ times the absolute value of the contact normal force $\mathbf{F}_N$,

$$|\mathbf{F}_T| \leq \mu |\mathbf{F}_N|. \tag{45}$$

The tangential contact force $\mathbf{F}_T$ opposes the relative velocity of roll and strip $(\mathbf{v} - \mathbf{v}_{\text{roll}})$,

$$\mathbf{F}_T = -\alpha(\mathbf{v} - \mathbf{v}_{\text{roll}}) \quad \text{with } \alpha \geq 0. \tag{46}$$

The velocity of the roll $\mathbf{v}_{\text{roll}}$ is determined by the angular velocity ω, the radius r, and the roll tangent $\mathbf{t}_{\text{roll}} = \mathbf{n}_{\text{roll}}^{\perp}$,

$$\mathbf{v}_{\text{roll}} = r\omega \mathbf{t}_{\text{roll}}. \tag{47}$$

In analogy to Eq. (6), the velocity of the strip in the contact point is given by

$$\mathbf{v}_c = \dot{\mathbf{p}}_c + v_0 \mathbf{p}_c'. \tag{48}$$

The quantities $\dot{\mathbf{p}}_c$ and $\mathbf{p}_c'$ denote the derivative of the position of the contact point with respect to t and $\bar{x}$, respectively. For the tangential, frictional contact model the cases of sticking and

slipping contact have to be distinguished. For both cases, the tangential contact force $\mathbf{F}_T$ will be applied in direction of the relative velocity of strip and roll $(\mathbf{v}_{\text{roll}} - \mathbf{v}_c)$.

To model the contact force in sticking points, a tangential creep velocity factor c_{cT} is used. Then, the contact force $\mathbf{F}_T$ is proportional to the relative velocity of strip and roll $(\mathbf{v}_{\text{roll}} - \mathbf{v}_c)$. This case applies as long as the tangential contact force is strictly smaller than the material friction coefficient μ times the absolute value of the contact normal force $\mathbf{F}_N$. Otherwise, the surfaces slide relatively. The absolute value of the tangential contact force reaches the bound $\mu|\mathbf{F}_N|$, the tangential force vector points in direction of the relative velocity $(\mathbf{v}_{\text{roll}} - \mathbf{v}_c)$. In summary, the tangential contact force vector is given by the relation

$$\mathbf{F}_T = \begin{cases} c_{cT} A_c (\mathbf{v}_{\text{roll}} - \mathbf{v}_c) & \text{if } |\mathbf{F}_T| \leq \mu |\mathbf{F}_N|, \\ \mu |\mathbf{F}_N| \frac{\mathbf{v}_{\text{roll}} - \mathbf{v}_c}{|\mathbf{v}_{\text{roll}} - \mathbf{v}_c|} & \text{else.} \end{cases} \tag{49}$$

In both cases, the respective negative tangential contact force $-\mathbf{F}_T$ is applied to the roll.

6 Computational results

As an example, a dynamic simulation of a belt drive is considered. Here, force is transmitted from a driving pulley to a second, free rotating pulley. The simulations were done using both standard ANCF Bernoulli–Euler beam elements and the beam elements with prescribed axial velocity proposed in this paper. With the new technique, the computational effort is reduced due to the fact that an adaptive discretization of the belt is possible, while the accuracy of the simulation was maintained. All implementations were done in the framework of the multibody dynamics simulation code HOTINT.[1]

6.1 Belt drive

As a model problem, a simulation of a belt drive is done using the proposed ANCF beam elements with prescribed axial velocity. The chosen example is taken from [4]. It consists of two pulleys and a flexible belt, which are modeled as rigid bodies and as ANCF Bernoulli–Euler beam, respectively. The setup is sketched in Fig. 4. Here, the left pulley is driven at a given angular velocity in positive direction. All data concerning the belt drive can be found in Table 1. Both pulleys are of radius $r = 0.09995$ m, the belt is of thickness $h_b = 0.01$ m and width $w_b = 0.08$ m. In initial, stress-free configuration the belt center line radius is given by $r_b = r + \frac{h_b}{2} = 0.10495$ m. The distance d between the two center points is set to $d = 0.1\pi$ m, thus the belt length in initial configuration is $l_b = 2r_b\pi + 0.2\pi = 0.4099\pi$ m. For force transmission, an initial tension of the belt is necessary. To this end, the position of the driving pulley is modified by a horizontal displacement $u_x = -0.0025$ m, which is applied linearly from beginning to time $t_0 = 0.05$ s.

The belt is assumed to have a Young modulus $E = 1 \times 10^7$ N/m^2 and a density of $\rho = 1036$ kg/m^3. The Young modulus is chosen this low in order to make the different angular velocities of driven and driver pulley noticeable.

For the driving pulley, an angular velocity $\omega_0 = 12$ rad/s is prescribed, which is applied linearly from time $t_0 = 0.05$ s to time $t_1 = 0.6$ s. The mass moment of inertia of the second pulley is given as $I_p = 0.25$ kg m^2.

[1] www.hotint.org.

Table 1 Data used in the numerical simulation of the belt drive

Parameter	Symbol	Value	Unit
radius pulley	r	0.09995	m
distance between pulleys	d	0.1π	m
belt thickness	h_b	0.01	m
belt width	w_b	0.08	m
belt length	l_b	0.4099π	m
horizontal displacement	u_x	-0.0025	m
Young's modulus	E	10^7	N/m^2
density	ρ	1036	kg/m^3
angular velocity of driving pulley	ω_0	12	rad/s
acceleration start time	t_0	0.05	s
acceleration end time	t_1	0.60	s
moment of inertia of driven pulley	I_p	0.25	kg/m^2
coefficient of friction	μ	1.2/0.5	–
contact stiffness	c_c	10^8	N/m^3
tangential contact stiffness	c_{cT}	10^7	kg/m^2 s

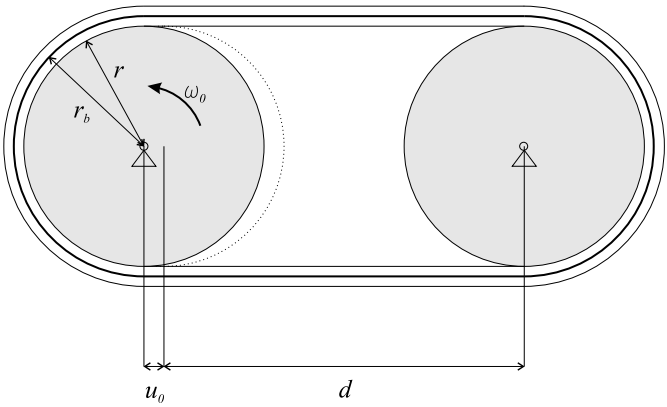

Fig. 4 Sketch of the belt drive. The left pulley is driven with given angular velocity ω_0, an initial tension of the band is achieved by the prescribed displacement u_0 of the driving pulley

Computations for two different coefficients of friction $\mu = 1.2$ and $\mu = 0.5$ are performed. The contact stiffness is chosen as $c_c = 10^8$ N/m^3 for the normal contact and $c_{cT} = 10^7$ kg/m^2 s for the tangential contact. Note that these values are higher than the values provided in [4] in order to obtain converged results.

Two computations were performed, where once standard ANCF Bernoulli–Euler elements from [5] were used, while for the second simulation elements with prescribed axial velocity were employed. The prescribed velocity is chosen as $v_0 = r_b\omega_0/|\mathbf{r}_0|$, where $|\mathbf{r}_0| = (l_b + 2|u_x|)/l_b$ is the axial stretch of the belt when the horizontal displacement u_x is applied to the driving pulley. The prescribed axial velocity evaluates to $v_0 = 1.2546434$ m/s. With this axial velocity, the intermediate configuration of the belt is almost constant in time. Thus, an adaptive discretization of the belt can be employed, using smaller elements in the contact zones near the rolls, and larger elements in the free-span regions, see Fig. 5 for a

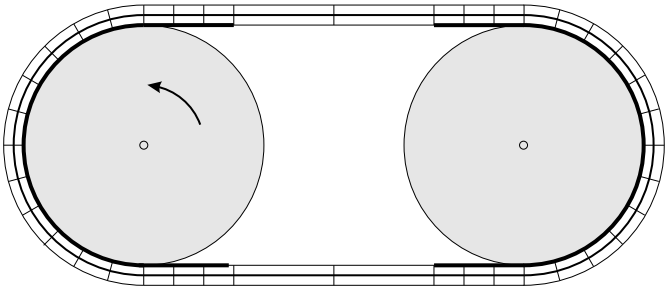

Fig. 5 Sketch of the discretization using axially moving elements. The contact zone is indicated at the belt surface

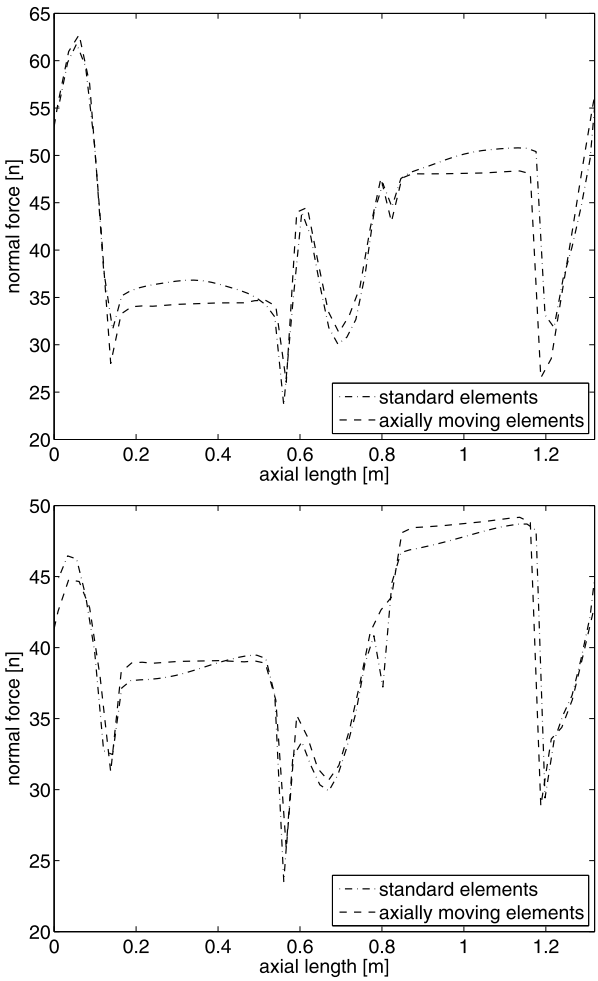

Fig. 6 Normal force as a function of the undeformed band length at end time $t_{\max} = 1$ s for discretization with standard ANCF Bernoulli–Euler elements and axially moving ANCF elements for different friction coefficients μ. *Top*: $\mu = 1.2$, *bottom*: $\mu = 0.5$

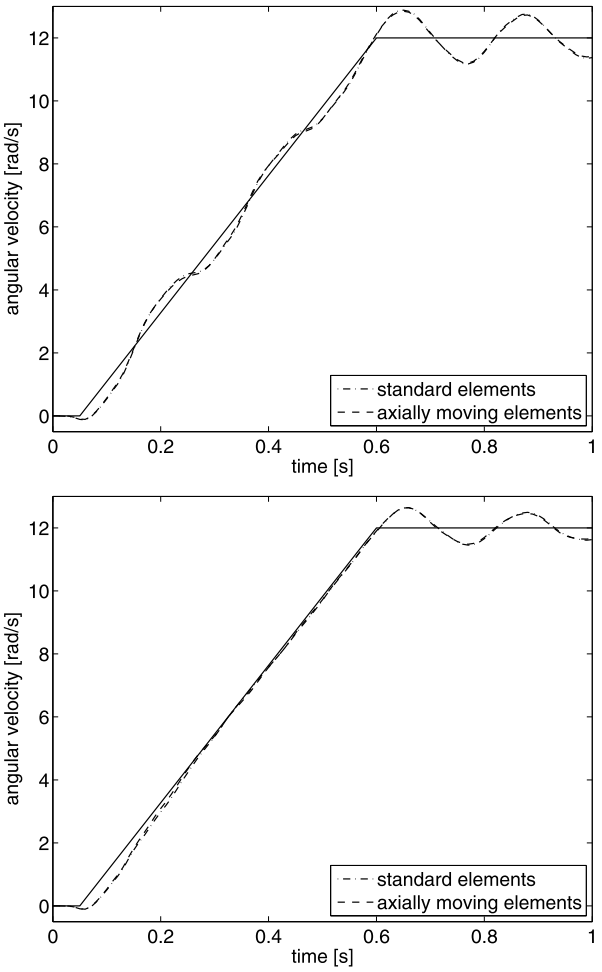

Fig. 7 Angular velocity of the driven pulley from time 0 to $t_{\max} = 1$ s for discretization with standard ANCF Bernoulli–Euler elements and axially moving ANCF elements for different friction coefficients μ. *Top*: $\mu = 1.2$, *bottom*: $\mu = 0.5$

sketch of the discretization and the contact zones. In case of standard Bernoulli–Euler elements, the whole belt has to be discretized by fine elements, as the contact zones vary in time. In the present example, in contact zones elements of approximate length 0.02 m were used, while for the axially moving elements in non-contact free-span areas, elements of length 0.1 m were used. This leads to a model consisting of 60 beam elements in the standard case, while only 40 axially moving elements were necessary for the same computational accuracy. The computational time dropped from approximately 595 s for standard elements to 350 s for axially moving elements. In Fig. 6, the normal force acting in the belt at the end time $t_{\max} = 1$ s is provided for both methods as a function of the undeformed beam axis. Figure 7 shows the angular velocity of the driven pulley over time for both methods. Note that during the first 0.1 s of the simulation a negative angular velocity of the driven pulley occurs, which is due to a small rotation of the pulley under the onset of gravity acting on the belt. The belt velocity over the undeformed belt length at end time is displayed in Fig. 8.

Additionally, computations with the lower contact stiffnesses from [4] $c_c = 10^7$ N/m^3 and $c_{cT} = 10^5$ kg/m^2 s were performed for a friction coefficient $\mu = 1.2$. In Fig. 9, the

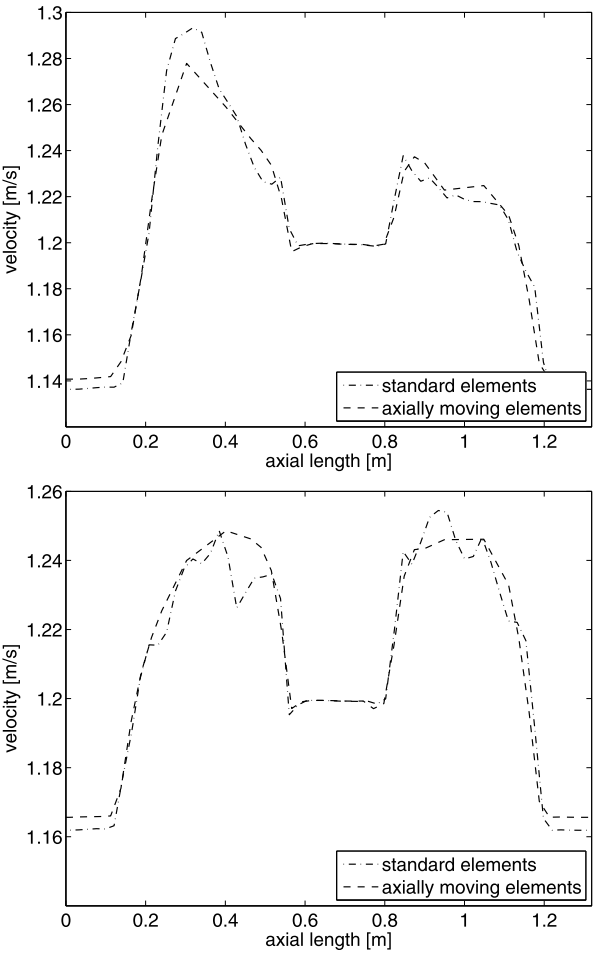

Fig. 8 Velocity as a function of the undeformed band length at end time $t_{\max} = 1$ s for discretization with standard ANCF Bernoulli–Euler elements and axially moving ANCF elements for different friction coefficients μ. *Top*: $\mu = 1.2$, *bottom*: $\mu = 0.5$

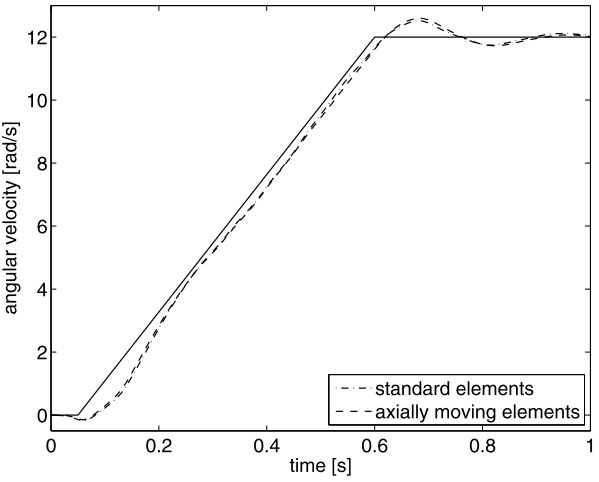

Fig. 9 Angular velocity of the driven pulley from time 0 to $t_{\max} = 1$ s for discretization with standard ANCF Bernoulli–Euler elements and axially moving ANCF elements for a friction coefficient $\mu = 1.2$ and contact stiffnesses as in Ref. [4]

angular velocities of the pulleys over time are displayed. Although one notices significant differences to the results from Fig. 7, the accordance with the results in [4] is good.

Acknowledgements The first author acknowledges support of the Austrian Science Fund FWF under project grant I 337-N18. The second author acknowledges support of the Comet-K2 Austrian Center of Competence in Mechatronics ACCM.

References

1. Behdinan, K., Stylianou, M.C., Tabarrok, B.: Dynamics of flexible sliding beams—non-linear analysis, part I: formulation. J. Sound Vib. **208**(4), 517–539 (1997)
2. Behdinan, K., Tabarrok, B.: Dynamics of flexible sliding beams—non-linear analysis, part II: transient response. J. Sound Vib. **208**(4), 541–565 (1997)
3. Berzeri, M., Shabana, A.: Development of simple models for the elastic forces in the absolute nodal co-ordinate formulation. J. Sound Vib. **235**(4), 539–565 (2002)
4. Dufva, K., Kerkkänen, K., Maqueda, L., Shabana, A.: Nonlinear dynamics of three-dimensional belt drives using the finite-element method. Nonlinear Dyn. **48**, 449–466 (2007). doi:10.1007/s11071-006-9098-9
5. Gerstmayr, J., Irschik, H.: On the correct representation of bending and axial deformation in the absolute nodal coordinate formulation with an elastic line approach. J. Sound Vib. **318**, 461–487 (2008)
6. Humer, A., Irschik, H.: Onset of transient vibrations of axially moving beams with large displacements, finite deformations and an initially unknown length of the reference configuration. Z. Angew. Math. Mech. **4**, 267–278 (2009)
7. Irschik, H., Holl, H.: The equations of Lagrange written for a non-material volume. Acta Mech. **153**, 231–248 (2002)
8. Shabana, A.: Definition of the slopes and the finite element absolute nodal coordinate formulation. Multibody Syst. Dyn. **1**, 248–339 (1997)
9. Simo, J.C., Vu-Quoc, L.: On the dynamics of flexible beams under large overall motions—the plane case: parts I and II. J. Appl. Mech. **53**, 849–863 (1986)
10. Sinwel, A., Gerstmayr, J.: Modeling an axially moving beam using the absolute nodal coordinate formulation. In: Topping, B.H.V., Adam, J.M., Pallarés, F.J., Bru, R., Romero, M.L. (eds.) Proceedings of the Seventh International Conference on Engineering Computational Technology. Civil-Comp Press, Stirlingshire (2010). doi:10.4203/ccp.94.112
11. Spelsberg-Korspeter, G., Kirillov, O.N., Hagedorn, P.: Modeling and stability analysis of an axially moving beam with frictional contact. J. Appl. Mech. **75**(3), 031001 (2008). doi:10.1115/1.2755166
12. Stangl, M., Gerstmayr, J., Irschik, H.: An alternative approach for the analysis of nonlinear vibrations of pipes conveying fluid. J. Sound Vib. **310**, 493–511 (2008)
13. Vu-Quoc, L., Li, S.: Dynamics of sliding geometrically-exact beams: large angle maneuver and parametric resonance. Comput. Methods Appl. Mech. Eng. **120**, 65–118 (1995)
14. Wickert, J.A., Mote, C.D.: Classical vibration analysis of axially moving continua. J. Appl. Mech. **57**(3), 738–744 (1990)